HHS Public Access

Author manuscript

Cancer Cell. Author manuscript; available in PMC 2017 July 11.

Published in final edited form as:

Cancer Cell. 2016 July 11; 30(1): 92–107. doi:10.1016/j.ccell.2016.05.008.

Epigenetic perturbations by Arg882-mutated DNMT3A potentiate aberrant stem cell gene expression program and acute leukemia development

Rui Lu[1,2], **Ping Wang**[3], **Trevor Parton**[1], **Yang Zhou**[4], **Kaliopi Chrysovergis**[5], **Shira Rockowitz**[6], **Wei-Yi Chen**[7], **Omar Abdel-Wahab**[8], **Paul A. Wade**[5], **Deyou Zheng**[3,6,*], and **Gang Greg Wang**[1,2,9,*]

[1]Lineberger Comprehensive Cancer Center, University of North Carolina School of Medicine, Chapel Hill, NC 27599, USA

[2]Department of Biochemistry and Biophysics, University of North Carolina School of Medicine, Chapel Hill, NC 27599, USA

[3]Department of Neurology, Albert Einstein College of Medicine, Bronx, NY 10461, USA

[4]Department of Pathology and Laboratory Medicine and McAllister Heart Institute, University of North Carolina School of Medicine, Chapel Hill, NC 27599, USA

[5]Laboratory of Molecular Carcinogenesis, National Institute of Environmental Health Sciences, National Institute of Health, Research Triangle Park, NC 27709, USA

[6]Department of Genetics, Albert Einstein College of Medicine, Bronx, NY 10461, USA

[7]Institute of Biochemistry and Molecular Biology, National Yang-Ming University, Taipei 11221, Taiwan

[8]Human Oncology and Pathogenesis Program, Memorial Sloan-Kettering Cancer Center, New York, NY 10065, USA

[9]Curriculum in Genetics and Molecular Biology, University of North Carolina at Chapel Hill, Chapel Hill, North Carolina 27599, USA

SUMMARY

[*]Correspondence author: deyou.zheng@einstein.yu.edu; Tel: 718-678-1217; greg_wang@med.unc.edu; Tel: 919-966-5952.

ACCESSION NUMBERS

The microarray, eRRBS-seq, and ChIP-seq data reported in this paper have been deposited to Gene Expression Omnibus (GEO) with an accession number GSE71475.

AUTHOR CONTRIBUTIONS

R.L. designed the research, performed experiments and computational analysis, interpreted data, and wrote the manuscript. P.W., S.R. and D.Z. performed computational analysis. T.P., Y.Z. and W.C. helped on animal modeling, viral transduction, and immunostaining studies, respectively. K.C. and P.A.W. participated in DNA methylome studies. O.A. helped on human AML cell studies. D.Z. supervised the computational studies. G.G.W. supervised the work, designed the research, interpreted data, and wrote the manuscript.

DNA methyltransferase 3A (*DNMT3A*) is frequently mutated in hematological cancers; however, the underlying oncogenic mechanism remains elusive. Here, we report that *DNMT3A* mutational hotspot at Arg882 (*DNMT3A*^{R882H}) cooperates with *NRAS* mutation to transform hematopoietic stem/progenitor cells and induce acute leukemia development. Mechanistically, DNMT3A^{R882H} directly binds to and potentiates transactivation of stemness genes critical for leukemogenicity including *Meis1, Mn1* and *Hoxa* gene cluster. DNMT3A^{R882H} induces focal epigenetic alterations, including CpG hypomethylation and concurrent gain of active histone modifications, at cis-regulatory elements such as enhancers to facilitate gene transcription. CRISPR/Cas9-mediated ablation of a putative *Meis1* enhancer carrying DNMT3A^{R882H}-induced DNA hypomethylation impairs *Meis1* expression. Importantly, DNMT3A^{R882H}-induced gene expression programs can be repressed through Dot1l inhibition, providing an attractive therapeutic strategy for *DNMT3A*-mutated leukemias.

Graphical Abstract

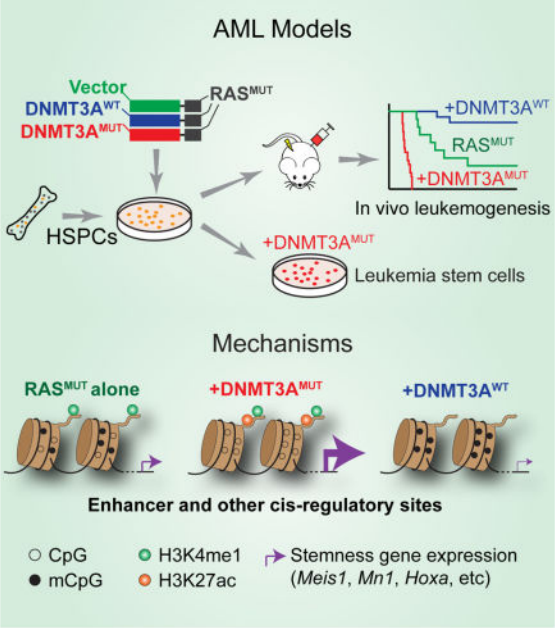

eTOC blurb/In Brief

Lu et al. establish that Arg882-mutated DNMT3A contributes to acute myeloid leukemia (AML) pathogenesis through epigenetic activation of leukemia-related genes. Inhibition of Dot1l reverses mutant DNMT3A-induced gene expression, indicating a potential therapeutic strategy for AMLs harboring this mutation.

INTRODUCTION

DNA methylation provides a critical epigenetic means for defining cellular identity and regulating functional output of gene-regulatory elements such as promoters and enhancers (Jones, 2012; Schubeler, 2015). Recently, DNA methyltransferase 3A (*DNMT3A*), a de novo DNA methyltransferase gene, was found mutated in ~20–30% of human acute myeloid

leukemias (AMLs) and ~10–20% of various other hematological cancers (Cancer Genome Atlas Research, 2013; Ley et al., 2010; Patel et al., 2012; Yan et al., 2011; Yang et al., 2015). *DNMT3A* mutations also associate well with clonally derived hematopoiesis at premalignant stages (Genovese et al., 2014; Jaiswal et al., 2014; Shlush et al., 2014; Xie et al., 2014) and often coexist with a secondary lesion that 'hits' either the FLT3-RAS kinase pathway, an epigenetic regulator (*IDH1/2, TET2*) or *NPM1* in AML patients (Cancer Genome Atlas Research, 2013; Ley et al., 2010; Patel et al., 2012; Yang et al., 2015). These clinical findings suggest that *DNMT3A* mutation acts as a founder lesion and requires additional genetic event to induce malignant development. Consistently, mice with *Dnmt3a* knockout in the bone marrow produced phenotypically normal hematopoietic stem cells (HSCs); only after rounds of transplantation did *Dnmt3a*-null HSCs display self-renewal advantages (Challen et al., 2012). Mice with *Dnmt3a* mutation alone did not develop frank AML but showed increased susceptibility to malignant development upon acquisition of additional mutations (Celik et al., 2015; Chang et al., 2015; Mayle et al., 2015; Xu et al., 2014).

Mutational hotspot at Arg882 (R882), a residue located within the homodimerization interface of DNMT3A, accounts for the majority (~60%) of *DNMT3A* mutations found in AMLs (Ley et al., 2010; Yang et al., 2015). Due to a primarily heterozygous nature of *DNMT3A* R882 mutation, it was thought to act in a dominant-negative and/or haploinsufficient manner (Holz-Schietinger et al., 2012; Kim et al., 2013; Russler-Germain et al., 2014). Clinical evidence supports this notion as AML patients with *DNMT3A* R882 mutation exhibited focal DNA hypomethylation (Russler-Germain et al., 2014). Despite these advances, there is a lack of relevant AML animal models for studying *DNMT3A* R882 mutation. Molecular pathways and mechanisms by which *DNMT3A* mutation contributes to AML pathogenesis remain undefined. Targeted approaches for the treatment of *DNMT3A*-mutated AMLs remain to be developed.

RESULTS

DNMT3A hotspot mutation enhances sensitivity of hematopoietic stem/progenitor cells (HSPCs) to transformation in vitro

Previous reports indicate that hotspot mutations of *DNMT3A* such as $DNMT3A^{R882H}$ act in a dominant-negative manner by disrupting formation of a DNMT3A-associated tetramer complex required for efficient DNA methylation (Holz-Schietinger et al., 2012; Kim et al., 2013; Russler-Germain et al., 2014). These studies prompted us to ask whether ectopic expression of human $DNMT3A^{R882H}$ in murine HSPCs could establish a transformation phenotype in a colony-forming unit (CFU) and replating assay (Figure S1A). Initially, we found a lack of CFU-promoting effect by $DNMT3A^{R882H}$ alone (Figures 1A–C). We then asked if $DNMT3A^{R882H}$ could enhance sensitivity of HSPCs to transformation in the presence of a second oncogenic lesion. Toward this end, we used a bicistronic retroviral system to coexpress either wild-type (WT) or R882H-mutant (RH) DNMT3A, together with other mutations known to coexist with *DNMT3A* mutation in human AMLs: either NRAS ($NRAS^{G12D}$), NPM1 (NPM1c), or IDH1 ($IDH1^{R132H}$) (Figure S1A) (Ley et al., 2010; Patel et al., 2012; Shih et al., 2012). Following viral transduction and drug selection, we obtained

highly pure HSPCs with comparable levels of oncogene expression for CFU assays (Figures 1C and S1B–C). We did not observe CFU-promoting effect of DNMT3A^{R882H} in the presence of NPM1c or IDH1^{R132H} (Figure S1D). However, a significant increase of CFUs was seen post-replating of HSPCs coexpressing DNMT3A^{R882H} and NRAS^{G12D} (hereinafter referred to as "RH-RAS"), relative to those with either oncogene alone (Figures 1A–B). In contrast to DNMT3A^{R882H}, DNMT3A^{WT} did not promote colony formation (Figure 1A–B). Post-replating, HSPCs expressing NRAS^{G12D} alone produced tiny and diffuse colonies of differentiated cells whereas those with RH-RAS gave rise to large, compact colonies that mainly comprised undifferentiated progenitors (Figures 1A insert, 1B and S1E–F). Importantly, cells expressing RH-RAS as derived from serially replated colonies were able to propagate and maintain their immature progenitor status in long-term liquid culture (Figures 1D and S1G), suggesting acquisition of indefinite self-renewal capability by these cells. These data have shown that, in contrast to DNMT3A^{WT}, R882-mutated DNMT3A promotes aberrant self-renewal of HSPCs and enhances their sensitivity to transformation in vitro. In addition, *NRAS^{G12D}* genetic background provides a useful platform for dissecting the role of *DNMT3A* mutation in AML development.

DNMT3A^{R882H} acts in concert with activated RAS to induce murine AMLs in vivo

The observed in vitro effect of DNMT3A^{R882H} on aberrant HSPC self-renewal and immortalization indicates that it could cooperate with NRAS^{G12D} to cause malignant transformation in vivo. Thus, we transplanted murine HSPCs freshly transduced with DNMT3A (either WT or RH) and/or NRAS^{G12D} to syngeneic mice. NRAS^{G12D} alone induced a myeloproliferative disease with incomplete penetrance (Figures 1E and S1H). DNMT3A^{R882H} alone did not cause detectable diseases over a 12-month monitoring period; however, in the presence of NRAS^{G12D}, it significantly accelerated development of leukemia with a shorter latency phenotype and full penetrance (Figure 1E). RH-RAS-induced leukemia was also characterized by hepatosplenomegaly (Figures 1F–G and S1I), leukemic infiltration to bone marrow, spleen and liver (Figures 1H and S1J), and elevated counts of peripheral white blood cells and blasts (Figures 1I, S1K–O and Table S1). Leukemia induced by RH-RAS expressed virally transduced genes at a level comparable to progenitors immortalized by RH-RAS in vitro (Figure 1J) and displayed an immature myeloid (AML) immunophenotype (Mac-1^{+}/c-Kit^{low}/Cd34^{low}/Gr1^{-}/Cd3e^{-}/Cd19^{-}/Ter119^{-}; Figures 1K, S1P–Q and Table S1). Whole-exome sequencing of 3 independent murine AMLs identified no recurrent mutation of additional genes (Figure S1R), suggesting that DNMT3A^{R882H} and NRAS^{G12D} are sufficient to drive AML development. Interestingly, unlike DNMT3A^{R882H}, DNMT3A^{WT} suppressed leukemogenesis in vivo (Figure 1E), suggesting that normal DNMT3A activities oppose AML pathogenesis.

DNMT3A hotspot mutation produces leukemia-initiating stem cells (LSCs) ex vivo in the presence of NRAS^{G12D}

To further verify cell transformation effect of RH-RAS, we used a previously described liquid cultivation system (Wang et al., 2007; Wang et al., 2009) and were able to recapitulate HSPC immortalization with RH-RAS only, and not either oncogene alone or coexpression of DNMT3A^{WT} with NRAS^{G12D} (Figure S2A). Similar to those derived from CFU assays, RH-RAS-immortalized progenitors stably maintained their progenitor identity in vitro in the

presence of SCF or Flt3 ligand, presented with expression of immature myeloid (c-Kit^{+}/Mac-1^{low}/Gr1^{-}) and stem cell antigens (Cd34^{low}/Flt3^{+}/Sca1$^{low/-}$) as well as a lack of other lineage markers (Figures 2A–B and S2B–C). Exposure of these progenitors to myeloid-promoting cytokines decreased cell proliferation (Figure S1G) and induced terminal myeloid differentiation (c-Kit^{-}/Mac-1^{high}/F4–80^{high}; Figures 2B and S2D), demonstrating their myeloid differentiation capability. Engraftment with each of 3 independent RH-RAS-immortalized progenitor lines induced murine AMLs (Figures S2E–H) that can be propagated in vivo with sequential transplantation (Figure 2C). Importantly, as few as 50–500 of these cells were sufficient to cause AML (Figure 2D), illustrating their LSC characteristic (hereinafter called "LSCs$^{RH\text{-}RAS}$"). To further characterize LSCs$^{RH\text{-}RAS}$, we profiled their transcriptome and genome-wide occupancy of H3K4me1, a histone mark demarcating lineage-specific enhancers (Lara-Astiaso et al., 2014). Unsupervised clustering of H3K4me1 profiles of LSCs$^{RH\text{-}RAS}$ and various hematopoietic cell lineages revealed a similarity of LSCs$^{RH\text{-}RAS}$ to HSPCs such as HSC and myeloid progenitors, when compared to differentiated cell types (Figures 2E and S2I); similar results were found in their transcriptome comparison (Figures 2F and S2J). Notably, a closer similarity was seen when comparing LSCs$^{RH\text{-}RAS}$ to leukemic progenitors we and others previously produced using either HOXA9 plus MEIS1 (Wang et al., 2005), MLL translocation (Bernt et al., 2011), NUP98-NSD1 (Wang et al., 2007) or NUP98-JARID1A (Wang et al., 2009) (Figures 2E and S2I–J), implying a commonality of pathways underlying leukemogenicity by these oncogenes.

R882-mutated DNMT3A potentiates abnormal transcription of stem cell genes including a Meis1-Mn1-Hoxa regulatory node

Next, we sought to understand the molecular basis underlying indefinite self-renewal shown by LSCs$^{RH\text{-}RAS}$. First, we asked if they carry self-renewal or stemness gene expression programs, a known feature of LSCs (Abramovich et al., 2005; Eppert et al., 2011; Krivtsov et al., 2006). By transcriptome analysis, we identified 54 genes uniquely expressed in LSCs$^{RH\text{-}RAS}$ and primitive HSPCs with self-renewal capabilities, relative to differentiating and mature hematopoietic cell types (Figure 3A and Table S2). The stem cell signature genes expressed in LSCs$^{RH\text{-}RAS}$ are only part of HSC stemness gene programs (~10%, Figure S3A); we further verified enrichment of the LSC$^{RH\text{-}RAS}$ stemness signature in self-renewing HSCs with independent datasets (Figures S3B–C). The top LSC$^{RH\text{-}RAS}$ stemness genes included *Hoxa9, Mn1, Hoxa5* and *Meis1* (Figure 3A), which encode a set of transcription factors (TFs) and cofactors crucial for sustaining self-renewal of normal HSCs and leukemic LSCs (Heuser et al., 2011; Huang et al., 2012; Wang et al., 2006; Wong et al., 2007). Gene targets of Meis1-Mn1-Hoxa, *Flt3* and *Sox4* (Heuser et al., 2011; Huang et al., 2012; Wang et al., 2005), were also among top stemness genes identified (Figure 3A), indicating activity of this TF regulatory circuitry in LSCs$^{RH\text{-}RAS}$. Moreover, activation of Meis1 and Hoxa in LSCs$^{RH\text{-}RAS}$ was found comparable to that in LSCs defined by other deregulated chromatin factors such as MLL-AF9, NUP98-JARID1A or NUP98-NSD1, while *Mn1* and *Mycn* showed unique expression in LSCs$^{RH\text{-}RAS}$ (Figures S3D–E).

As LSCs$^{RH\text{-}RAS}$ carry both *DNMT3A* and *NRAS* mutations, we next asked what stemness gene signatures are dependent on *DNMT3A*^{R882H}. We performed microarray studies using

HSPCs post-transduction of $NRAS^{G12D}$ alone or with coexpressed DNMT3A, either WT or R882H-mutant (hereinafter refer as EV-RAS, WT-RAS or RH-RAS). These HSPCs were collected 12 and 16 days after viral transduction when their proliferation rates were comparable (Figure S2A). Among the 54 $LSC^{RH\text{-}RAS}$ stemness genes, 9 were found upregulated by $DNMT3A^{R882H}$ at both time points, including *Meis1*, *Mn1* and *Hoxa* (Figures 3B and S3F). Consistently, Gene Set Enrichment Analysis (GSEA) found that gene sets associated with AML development, undifferentiated myeloid cells, and NUP98-HOXA9 targets were significantly enriched in HSPCs with RH-RAS (Figure 3C). Conversely, gene sets associated with myeloid differentiation showed reduced expression in HSPCs expressing RH-RAS, relative to EV-RAS (Figure 3D), whereas the same gene sets showed enhanced expression in HSPCs expressing WT-RAS (Figure 3D), thus suggesting opposite effects of WT and R882-mutated DNMT3A on regulating genes crucial for HSPC self-renewal versus differentiation. We verified unique upregulation of *Meis1*, *Hoxa* and *Mn1* in RH-RAS HSPCs (Figures 3E and S3G) and their induced AMLs (Figures 3F–G and S3H). To functionally assess whether the activated Meis1-Mn1-Hoxa circuitry is essential for RH-RAS-induced AML development, we introduced independent small hairpin RNAs (shRNAs) of *Meis1* or *Mn1* into $LSCs^{RH\text{-}RAS}$ (Figure 3H) and found that knocking down either gene significantly impaired in vitro growth of $LSCs^{RH\text{-}RAS}$ (Figures 3I and S3I) as well as their in vivo leukemogenic function (Figures 3J and S3J–K).

Together, these data reveal a role of R882-mutated *DNMT3A* in potentiating abnormal activation of stemness genes such as *Meis1, Mn1* and *Hoxa*, which are required for mutant DNMT3A-mediated AML progression.

ChIP-Seq reveals context-dependent targeting of R882-mutated DNMT3A into the LSC genome

The $LSC^{RH\text{-}RAS}$ cellular model described above provides an ideal system for dissecting the molecular mechanism underlying $DNMT3A^{R882H}$-mediated oncogenesis. Mutant DNMT3A proteins are exclusively nuclear (Figure S4A), thus, we first mapped their genome-wide occupancy in $LSCs^{RH\text{-}RAS}$ by ChIP-Seq using antibodies against the Myc tag fused to $DNMT3A^{R882H}$ (Figure S1A). Myc-$DNMT3A^{R882H}$ ChIP-Seq gave robust and specific signals (Figure 4A); as a negative control, Myc ChIP-Seq using cells without Myc-$DNMT3A^{R882H}$ expression did not detect any peaks (Figure S4B). We identified 13,705 genomic regions with significant $DNMT3A^{R882H}$ binding (i.e. $DNMT3A^{R882H}$ peaks, Table S3) in $LSCs^{RH\text{-}RAS}$, which spread over promoter and inter- or intra-genic regions (Figure S4C). $DNMT3A^{R882H}$ exhibited a broad binding pattern with an average peak size of ~17 kb (Figures S4D and 4B, with an example peak at *Lig1*). Interestingly, $DNMT3A^{R882H}$ binding was stronger at intermediately transcribed genes, relative to low or highly expressed genes (Figure 4A), and positively correlated to CpG dinucleotide density except at CpG islands (CGIs) where $DNMT3A^{R882H}$ has a sharp drop in overall binding (Figure 4C). $DNMT3A^{R882H}$ binding regions also showed depletion of H3K4me3 (Figures 4D), a histone modification known to suppress DNMT3A binding due to an intrinsic histone H3-'reader' activity of DNMT3A's ADD domain (Guo et al., 2015; Noh et al., 2015). Intriguingly, 76.1% of $DNMT3A^{R882H}$ peaks were found in close proximity to and significantly overlapped with peaks of H3K4me1, a histone mark demarcating enhancer elements

(observed/expected = 10.2, p < 1e-300; Figure 4E), as exemplified by those identified in an intron region of *Lig1* and an intergenic region of *Vegfa* (Figures 4B, insert, and S4E, boxed areas). Ontology analysis of DNMT3A^{R882H} peaks revealed their significant enrichment at genes related to normal and malignant hematopoiesis, PML-RARα targets and *MLL* rearrangement-associated genes (Figures 4F and S4F). Notably, key AML-promoting or stemness genes upregulated by DNMT3A^{R882H} such as *Meis1, Mn1, Hoxa* and *Mycn* were all found directly bound by DNMT3A^{R882H} (Figures 4G–H and S4G–H). Collectively, our genome-wide profiling of DNMT3A^{R882H} has revealed a CpG content and 'histone code'-dependent targeting of R882-mutated DNMT3A into cancer cell genomes; we have also identified a previously unappreciated overlap of DNMT3A^{R882H} with putative enhancer and cis-regulatory sites (marked by H3K4me1) at numerous developmental genes including a Meis1-Mn1-Hoxa node.

R882-mutated DNMT3A induces focal hypomethylation of CpG sites enriched with gene-regulatory elements

We next aimed to delineate DNMT3A^{R882H}-induced epigenetic perturbations during AML progression. By enhanced Reduced Representation Bisulfite Sequencing (eRRBS), we mapped global DNA methylation patterns of murine HSPCs 16 days post-transduction of EV-RAS, RH-RAS or WT-RAS. Analysis of eRRBS data, which had 11–12× coverage for 6.5 million CpGs in all samples, revealed no significant changes in global CpG methylation (Figure S5A–C) except a moderate change at CpG shores (Figure S5C). By pairwise comparison of CpG methylation, we identified 12,889 differentially methylated CpG sites (DMCs) in HSPCs expressing RH-RAS relative to EV-RAS, with most of DMCs (80.8%) hypomethylated (Figure 5A, left; hereinafter called as "DNMT3A^{R882H}-associated hypo-DMCs"); in contrast, DMCs associated with DNMT3A^{WT} are largely hypermethylated (hyper-DMCs, 80.6%; Figure 5A, right). DNMT3A^{R882H}-associated hypo-DMCs were found mainly in intron, intragenic and promoter regions, while DNMT3A^{WT}-induced hyper-DMCs were enriched in promoters and CGIs (Figures S5D–E). Importantly, DNMT3A^{R882H}-associated hypo-DMCs were significantly enriched at genomic regions with H3K4me1 (Figure 5B) or with DNMT3A^{R882H} binding (Figure 5B–C). DNMT3A^{R882H}-associated hypo-DMCs were also found enriched with the binding site of the ETS family of TFs (Erg and Spi1/PU.1) and other hematopoietic TFs (Runx1 and Mycn; Figure 5D). In contrast, DNMT3A^{R882H}-associated hyper-DMCs exhibited none of these features and, instead, correlated negatively to DNMT3A^{R882H} binding (Figures 5B–5D), suggesting that creation of hyper-DMCs is due to indirect effect of DNMT3A^{R882H}.

Consistent with DMCs, differentially methylated regions (DMRs) identified in HSPCs co-transduced with DNMT3A^{R882H} relative to control were mainly hypomethylated (hereinafter called "DNMT3A^{R882H}-associated hypo-DMRs"; Table S4, n = 1,199) while DNMT3A^{WT}-associated DMRs were mainly hypermethylated (hyper-DMRs) (Figures 5E and S5F). These two sets of DMRs showed a significant overlap, including those found at DNMT3A^{R882H}-deregulated stemness genes (*Meis1, Mn1, Hoxa7* and *Mycn)*, further highlighting that WT and R882-mutated DNMT3A have opposing effects on DNA methylation of crucial AML-promoting genes (Figure 5F). In addition, DNMT3A^{R882H}-associated hypo-DMRs were enriched at genes related to transcriptional regulation,

hematopoietic development and cancer (Figures 5G and S5G). Consistent with results in DMCs, H3K4me1 and DNMT3A^{R882H} binding were significantly enriched at DNMT3A^{R882H}-associated hypo-DMRs (Figures 5H and S5H). Taken together, our results show that R882-mutated DNMT3A is sufficient to induce CpG hypomethylation at putative cis-regulatory sites of key stemness genes that we have functionally validated as essential for AML progression in murine models.

DNMT3A^{R882H}–induced DNA hypomethylation identified in murine models mirrors what was seen in human AMLs with *DNMT3A* R882 mutation

A focal CpG hypomethylation phenotype seen in the above murine model is reminiscent of what was observed in human AMLs with *DNMT3A* mutation (Russler-Germain et al., 2014). To assess whether our murine model mimics human disease, we first identified regions in the human genome that are homologous (i.e., conserved) to DNMT3A^{R882H}-associated hypo-DMRs defined in the murine model. We then found that, relative to randomized control, CpGs located in such conserved human genomic sites showed a significant reduction in their methylation levels among human AML samples with *DNMT3A* R882 mutation, relative to those with normal *DNMT3A* (Figure 5I; $p < 2.2e\text{-}16$). Despite a relatively limited coverage of CpGs by the 450K-array platform used in the human AML study (Russler-Germain et al., 2014), genes with hypo-DMRs identified in AML patients carrying *DNMT3A* R882 mutation also had significant overlap with those that gain DNMT3A^{R882H}-associated hypo-DMRs in our murine model (Table S5; $p < 0.05$). We identified 119 genes showing CpG hypomethylation in both human AMLs and murine LSC models, which again include stemness and AML-promoting genes *MEIS1, HOXA7* and *MN1* (Figures 5J and S5I). We subsequently verified differential CpG methylation of DMRs at these genes in murine cells by direct bisulfite sequencing (Figures 5K and S5J), and further showed that a consistent hypomethylation pattern exists at conserved DMRs in human AMLs with *DNMT3A* R882 mutation, relative to those with non-R882 mutated or normal *DNMT3A* (Figures 5L and S5K).

Hypo-DMRs induced by DNMT3A^{R882H} facilitate gain of histone acetylation at gene-regulatory sites

Because DNMT3A^{R882H} binding and induced hypo-DMRs showed significant overlap with H3K4me1, a histone mark demarcating gene-regulatory regions such as enhancers and proximal elements close to promoters (Rada-Iglesias et al., 2011), we performed ChIP-Seq profiling of H3K27ac, a histone modification correlating to enhancer/promoter activity, with the samples we used for eRRBS. Intriguingly, we found that introducing DNMT3A^{R882H} to HSPCs caused an overall gain of H3K27ac at DNMT3A^{R882H}-associated hypo-DMRs (Figure 6A, left) whereas no overall change in H3K4me1 was seen for these hypo-DMRs (Figure 6B, left); in contrast, expression of DNMT3A^{WT} decreased overall H3K27ac and H3K4me1 at these hypo-DMRs (Figures 6A and 6B, left). As a control, DNMT3A^{R882H}-associated hyper-DMRs did not show such changes (Figures 6A and 6B, right). Consistently, similar histone modification changes were seen at regions in close proximity to DNMT3A-associated DMCs (Figures S6A and S6B). Importantly, DMRs at key stemness or AML genes such as *Meis1, Mn1, Hoxa and Mycn* all exhibited significant gain of H3K27ac in DNMT3A^{R882H}-expressing HSPCs as well as loss of H3K27ac in DNMT3A^{WT}-expressing

HSPCs at their putative cis-regulatory sites (Figures 6C and S6C–S6H). By ChIP-qPCR, we verified the observed changes of H3K27ac and H3K4me1 at a panel of DMRs post-transduction of DNMT3A^{R882H} versus DNMT3A^{WT} into HSPCs (Figures 6D and S6I). Furthermore, expression of DNMT3A^{R882H} enhanced binding of the H3K27 acetyltransferase p300 to hypo-DMRs at stemness genes (Figure 6E), suggesting that CpG hypomethylation facilitates recruitment of H3K27ac 'writers'. In addition, overall gain of H3K27ac at hypo-DMRs was found significant regardless of expression changes of their associated genes (Figure S6J), indicating that H3K27ac gain at hypo-DMRs is not merely a consequence of gene activation, as exemplified by that found at hypo-DMRs of *Kdm2b, Sirt4* and *Pax5* (Figures S6K–S6M).

Because DNMT3A^{R882H}-induced hypo-DMRs can be found outside of gene-regulatory regions, we have focused on those overlapping with a peak of H3K4me1 (a total of 777 DMRs) or H3K27ac (333 DMRs) in at least one cell condition and found that, in either case, 9 to 11-fold more of DMRs showed enhanced H3K27ac levels than those with decreased H3K27ac (Figure 6F). These results indicate that DNA hypomethylation facilitates H3K27ac gain at gene-regulatory sites but also acts in a context-dependent manner. Consistently, more hypo-DMRs with gained H3K27ac were observed at regions showing a greater loss of CpG methylation (Figure 6G), supporting degree of DNA hypomethylation as a contributing factor that fine-tunes functional output of gene-regulatory sites. Moreover, genes with increased H3K27ac at their hypo-DMRs were found enriched in HSPCs expressing RH-RAS relative to EV-RAS (Figures 6H), from which we identified 57 genes as both epigenetically altered and transcriptionally activated by DNMT3A^{R882H} (thus hereafter called as "DNMT3A^{R882H} signature genes", Figure 6I and Table S6). Notably, these DNMT3A^{R882H} signature genes included DNMT3A^{R882}-associated stemness genes we have studied above (a *Meis1-Mn1-Hoxa* node and *Mycn*) as well as other putative AML-promoting genes such as *Id2, Bcl2* and *Runx3* (Figure 6I).

The *Meis1* intron 6 enhancer carrying DNMT3A^{R882H}-induced CpG hypomethylation is crucial for *Meis1* gene activation in LSCs

To demonstrate a causal role of DNMT3A^{R882H}-induced focal DNA hypomethylation in gene expression regulation, we cloned sequences from a panel of hypo-DMRs into a CpG-free reporter system designed to assess putative gene-regulatory activity and its relationship to CpG methylation (Schmidl et al., 2009). We found all tested hypo-DMRs possess strong expression-enhancing activity in the absence of their CpG methylation (Figure 6J). CpG methylation of these hypo-DMRs completely abolished their expression-enhancing activities (Figure 6J), demonstrating a hypomethylation-dependent activation of cis-regulatory elements harbored within hypo-DMRs. To further verify DMR-associated enhancer activity in LSCs^{RH-RAS}, we closely examined a hypo-DMR located in the intron 6 of *Meis1* (Figure 6C, green bar) because *Meis1* is a critical effector gene for DNMT3A^{R882H}-associated AML progression (Figures 3H–3J) and this hypo-DMR is also found conserved in human AMLs with *DNMT3A* R882 mutation (Figures 5J–5L). Notably, this hypo-DMR is positive for H3K4me1 (Figure 6C) and has a significant overlap with a previously reported *MEIS1* enhancer in human cells (Xiang et al., 2014). First, we carried out Chromosome Conformation Capture (3C), a surrogate assay for scoring enhancer usage and promoter

association, and indeed detected a long-range looping interaction of the intron 6 hypo-DMR with the *Meis1* promoter in LSCs$^{RH\text{-}RAS}$ (Figure 6K). To further determine the role of this putative intron 6 enhancer in DNMT3A^{R882H}-induced *Meis1* gene activation, we employed the CRISPR/Cas9-based genomic editing technology. Cas9 and a pair of single guide RNAs (sgRNA) targeting boundaries of the *Meis1* hypo-DMR were transduced into LSCs$^{RH\text{-}RAS}$ (Figure 6L). PCR and direct sequencing confirmed sgRNA-mediated specific deletion of the hypo-DMR in five independent LSC$^{RH\text{-}RAS}$ lines (Figures 6M–6N and S6N). In all cases, ablation of this putative enhancer significantly reduced *Meis1* expression (Figure 6O). Consistently, among human AMLs with *DNMT3A* R882 mutation, lower DNA methylation at the *MEIS1* intron 6 correlated with higher expression of *MEIS1* (Figure 6P). It is also worth noting that 54.5% (6/11) of *DNMT3A* WT AMLs display significant DNA methylation of *MEIS1* intron 6 and yet express *MEIS1* at high levels (Figure 6P), indicating different gene activation mechanisms exist in these AML cases. Together, using *Meis1* as a paradigm example, we show that focal CpG hypomethylation induced by DNMT3A R882 mutation promotes enhancer activation and expression of key AML genes.

Dot1l inactivation suppresses DNMT3A^{R882H}-associated LSC properties and aberrant activation of stemness gene programs

To explore the potential strategy for reversing DNMT3A^{R882H}-induced gene deregulation and thus treating *DNMT3A*-mutated leukemia, we conducted compound treatment studies with a collection of epigenetic regulator inhibitors and identified that LSCs$^{RH\text{-}RAS}$ showed a significantly higher sensitivity to a Dot1l inhibitor, SGC0946, relative to control cells without *DNMT3A* mutation, i.e. LSCs expressing *NRAS^{G12D}* plus oncogenic TFs (Figure S7A). Dot1l, a histone H3 lysine 79 (H3K79) methyltransferase, belongs to a transcription elongation regulatory complex that engages acetylated histones at cis-regulatory sites (Li et al., 2014). Genomic profiling of H3K79 dimethylation (H3K79me2) detected its overall elevation at DNMT3A^{R882H}-associated hypo-DMRs in HSPCs (Figure 7A), as exemplified by those at *Meis1, Hoxa, Mn1* and *Mycn* (Figures 7B and S7B). We confirmed H3K79me2 gain at these genes by ChIP-qPCR (Figure S7C). Next, we asked if pharmacological inhibition of Dot1l could reverse DNMT3A^{R882H}-induced gene activation. We first confirmed SGC0946-mediated suppression of H3K79me2 in LSCs$^{RH\text{-}RAS}$ (Figure S7D), followed by microarray profiling. Notably, after SGC0946 treatment, we detected significant downregulation of DNMT3A^{R882H} signature genes (Figures 7C and 7D) and concurrent upregulation of myeloid differentiation genes in LSCs$^{RH\text{-}RAS}$ (Figures 7D and S7E). Although *Hoxa* and *Meis1* were shown as part of MLL-AF9 target genes that are dependent on Dot1l (Chen et al., 2015), the DNMT3A^{R882H} signature genes displayed a greater sensitivity to Dot1l inhibitors than MLL-AF9 targets in LSCs$^{RH\text{-}RAS}$ (Figure 7E); conversely, the DNMT3A^{R882H} signature genes do not show overall response to Dot1l inhibitors in MLL-AF9-transformed AML cells (Figure S7F). These analyses indicate that *DNMT3A* R882 mutation confers a unique dependency on the Dot1l enzymatic activity in AML. We further verified downregulation of DNMT3A^{R882H}-associated stemness genes *Hoxa, Meis1, Mn1* and *Mycn* after treatment with SGC0946 (Figures 7F and 7G and S7G) or knockdown of Dot1l (Figures 7H and S7H and S7I). In response to Dot1l inactivation, multiple murine and human AML lines bearing *DNMT3A* mutation showed suppressed in vitro growth (Figures 7I and S7J and S7K) and concurrent cell differentiation (Figures 7J

and 7K and S7L–S7N). *DNMT3A*-mutated human AML lines also had decreased *HOXA* or *MEIS1* expression upon DOT1L blockade (Figures S7O and S7P). In contrast, various murine and human leukemia lines established by oncogenic TFs were all insensitive to Dot1l inhibition (Figures 7I and S7K). Also, enforced expression of HOXA9 plus MEIS1 reversed sensitivity of $LSCs^{RH\text{-}RAS}$ to Dot1l inhibition (Figure 7L), demonstrating a crucial role of these TFs in $DNMT3A^{R882H}$-mediated oncogenic effects. Importantly, knockdown of Dot1l in $LSCs^{RH\text{-}RAS}$ or their pre-treatment with Dot1l inhibitors significantly delayed in vivo AML progression and prolonged survival of engrafted mice (Figure 7M). Collectively, we show that expression of $DNMT3A^{R882H}$ confers Dot1l dependency in AML and that reversing $DNMT3A^{R882H}$-induced gene activation by Dot1l inhibition may provide a potential therapeutic means for the treatment of AMLs with *DNMT3A* mutation.

DISCUSSION

In this study, we report a set of ex vivo LSC and in vivo murine AML model systems for studying functionality of *DNMT3A* R882 mutation in AML pathogenesis. Using these human disease-mimicking models, we have (1) defined a causal role of $DNMT3A^{R882H}$ in promoting AML transformation in vitro and in vivo; (2) identified $DNMT3A^{R882H}$-deregulated gene pathways, including a Meis1-Mn1-Hoxa TF node that we functionally validated as essential for $DNMT3A^{R882H}$-mediated AML progression; (3) shown that $DNMT3A^{R882H}$ directly binds to gene-regulatory sites, notably enhancers, inducing focal DNA hypomethylation and concurrent gain of histone acetylation; (4) determined a critical role of the epigenetically altered enhancer and cis-regulatory elements for $DNMT3A^{R882H}$-associated gene activation; and (5) importantly, we have also demonstrated that pharmacological inhibition of Dot1l reverses the mutant DNMT3A-associated gene activation, thus providing a potential therapeutic avenue for the affected AMLs.

The molecular pathways identified in this study help explain several important biological phenomena related to *DNMT3A* mutation and hematological disease. First, as the Meis1-Mn1-Hoxa circuitry is crucial for both normal expansion of HSCs and malignant transformation of LSCs (Argiropoulos and Humphries, 2007; Heuser et al., 2011), deregulation of this TF node by R882-mutated DNMT3A provides a molecular explanation not only for malignant hematopoiesis but also for clonal hematopoiesis, a phenotype strongly associated with *DNMT3A* mutation (Genovese et al., 2014; Jaiswal et al., 2014; Xie et al., 2014). In addition, these findings help explain a mutually exclusive pattern for *DNMT3A* mutation and *MLL* rearrangement in AMLs (Cancer Genome Atlas Research, 2013; Patel et al., 2012) because the latter itself is a strong inducer of *Meis1* and *Hoxa* activation (Chi et al., 2010).

Our results also demonstrate requirement of cooperation between *DNMT3A* mutation and the activated kinase such as RAS for AML induction. RAS mutation alone induces an hyper-proliferative phenotype but does not support self-renewal, which is in agreement with previous studies (Zhang et al., 2009); RAS activation was also known to induce cell senescence, a barrier of cancer development (Campisi and d'Adda di Fagagna, 2007). On the other hand, *DNMT3A* mutation confers aberrant HSPC self-renewal, blocks differentiation programs and yet lacks pro-proliferation effect; besides a Meis1-Mn1-Hoxa node we have

functionally confirmed as essential for DNMT3A^{R882H}-associated AML, other downstream targets of DNMT3A^{R882H}, such as pro-survival (*Bcl2*), anti-differentiation (*Id2*) and stemness (*Mycn*) genes, might be equally crucial for AML progression. These findings suggest that synergy between DNMT3A and kinase mutations is likely due to their differential effects on pathways relating to AML development. However, it is also possible that the two mutations may affect distinctive sets as well as same sets of downstream effectors via genetic or epigenetic mechanisms. A similar synergy is most likely to exist between *DNMT3A* mutation and the activated FLT3, which acts upstream of RAS and coexists with the former in human AMLs as well.

Our studies clearly show that *DNMT3A* mutation-induced CpG hypomethylations are not random: they are significantly enriched at gene-regulatory sites, notably, putative enhancers marked by H3K4me1 as well as the binding sites of master hematopoietic TFs. Precise mechanisms by which CpG methylation of these cis-regulatory sites regulates gene expression remain to be fully studied. For example, despite a large number of DMCs found associated with either *DNMT3A* or *TET2* mutation in AML, a relatively small number of genes show changes in their expression (Russler-Germain et al., 2014; Shih et al., 2015). A possible explanation is that effect of CpG methylation on gene expression is context dependent (Baubec and Schubeler, 2014): degree of CpG methylation change, density or genomic location of CpG, methyl-CpG “readers” and TF binding are all possible factors affecting the ultimate effect of DNA methylation on gene expression. Unlike histone (de)acetylation, CpG (de)methylation at distal cis-regulatory sites such as enhancers may act as a permissive mechanism influencing gene expression, rather than a strong and instructive one controlling levels of gene activation and transcription. Nevertheless, using reporter assays and CRISPR/Cas9-mediated enhancer editing, we have determined the role of select hypo-DMRs in activation of associated target genes such as *Meis1*.

This study also provides useful information on how to treat *DNMT3A*-mutated AMLs. Pharmacological blockade of Dot1l reversed *DNMT3A* mutation-induced gene activation resulting in an impaired AML pathogenesis. In the future, examination of other ‘druggable’ factors would likely identify additional therapeutic strategies for the treatment of *DNMT3A*-mutated AMLs. Therefore, in addition to elucidating the underlying oncogenic mechanisms, the ex vivo and in vivo model systems presented herein should be useful for exploring AML therapeutics.

EXPERIMENTAL PROCEDURES

In vitro colony-forming unit (CFU) assay with serial replating

Following lineage-negative (Lin$^-$) enrichment and retroviral transduction, 30,000 of infected HSPCs were plated in the semi-solid methylcellulose cultivation system (Methocult, Stem Cell Technologies), followed by CFU counting and replating for every 10–14 days according to manufacturer’s protocol.

Animal studies and In vivo leukemogenic assay

All animal experiments were approved by and performed in accord with the guidelines of the Institutional Animal Care and Use Committee at the University of North Carolina (Chapel Hill, NC). Leukemogenic potentials of transduced HSPCs were evaluated by BMT into sublethally irradiated syngeneic mice. Briefly, 200,000 of bone marrow-derived Lin^- HSCPs following procedures of cytokine stimulation, retroviral transduction and drug selection were injected via tail veil to recipient mice as described before (Wang et al., 2009).

Statistical Analysis

Data are presented as the mean ± SD for 3 independent experiments unless otherwise noted. Statistical analysis was performed with Student's t-test for comparing two sets of data with assumed normal distribution. We used Mann-Whitney U test for data not showing a normal distribution, chi-square test for categorical variables, and log-rank test for Kaplan-Meier survival curves to determine statistical significance. A p value < 0.05 was considered significant.

The detailed procedures of plasmid construction, cell culture, antibody and immunoblot, flow cytometry, microarray analysis, ChIP-Seq, eRRBS, Exome-Seq, RT-qPCR, ChIP-qPCR, 3C-qPCR, shRNA-mediated knockdown, luciferase reporter assay, CRISPR/Cas9-mediated genomic editing, as well as the detailed information for computational and statistical analysis of deep sequencing data, are described in Supplemental Experimental Procedures.

Supplementary Material

Refer to Web version on PubMed Central for supplementary material.

Acknowledgments

We graciously thank Drs. Y. Xiong and K. Humphries for providing constructs, M. Kamps and M. Minden for leukemia lines, M. Torres for Meis1 antibody, D. Bauer and F. Zhang for CRISPR/Cas9 systems, M. Rehli for a CpG-free reporter, and J. Bear for an shRNA vector used in this study. Thanks to Drs. D. Allison and L. Cai and other members of the Wang laboratory for helpful discussion and technical support. We thank UNC's Genomics Core, Animal Studies Core, Flow Core, and HTSF core for their supports of this work. This work is supported by NCI K99/R00 grant CA151683 to G.G.W., a DoD grant CA130247 to G.G.W., and grants of Gabrielle's Angel Foundation to O.A. and G.G.W. G.G.W. is an American Society of Hematology (ASH) Scholar and a Kimmel Scholar. R.L. is a Lymphoma Research Foundation Postdoc Fellow. UNC Cores including flow cytometry facility are supported in part by the North Carolina Biotech Center Institutional Support Grant (2012-IDG-1006) and UNC Cancer Center Core Support Grant (P30 CA016086).

References

Abramovich C, Pineault N, Ohta H, Humphries RK. Hox genes: from leukemia to hematopoietic stem cell expansion. Annals of the New York Academy of Sciences. 2005; 1044:109–116. [PubMed: 15958703]

Argiropoulos B, Humphries RK. Hox genes in hematopoiesis and leukemogenesis. Oncogene. 2007; 26:6766–6776. [PubMed: 17934484]

Baubec T, Schubeler D. Genomic patterns and context specific interpretation of DNA methylation. Current opinion in genetics & development. 2014; 25:85–92. [PubMed: 24614011]

Bernt KM, Zhu N, Sinha AU, Vempati S, Faber J, Krivtsov AV, Feng Z, Punt N, Daigle A, Bullinger L, et al. MLL-rearranged leukemia is dependent on aberrant H3K79 methylation by DOT1L. Cancer cell. 2011; 20:66–78. [PubMed: 21741597]

Campisi J, d'Adda di Fagagna F. Cellular senescence: when bad things happen to good cells. Nat Rev Mol Cell Biol. 2007; 8:729–740. [PubMed: 17667954]

Cancer Genome Atlas Research N. Genomic and epigenomic landscapes of adult de novo acute myeloid leukemia. The New England journal of medicine. 2013; 368:2059–2074. [PubMed: 23634996]

Celik H, Mallaney C, Kothari A, Ostrander EL, Eultgen E, Martens A, Miller CA, Hundal J, Klco JM, Challen GA. Enforced differentiation of Dnmt3a-null bone marrow leads to failure with c-Kit mutations driving leukemic transformation. Blood. 2015; 125:619–628. [PubMed: 25416276]

Challen GA, Sun D, Jeong M, Luo M, Jelinek J, Berg JS, Bock C, Vasanthakumar A, Gu H, Xi Y, et al. Dnmt3a is essential for hematopoietic stem cell differentiation. Nature genetics. 2012; 44:23–31. [PubMed: 22138693]

Chang YI, You X, Kong G, Ranheim EA, Wang J, Du J, Liu Y, Zhou Y, Ryu MJ, Zhang J. Loss of Dnmt3a and endogenous Kras(G12D/+) cooperate to regulate hematopoietic stem and progenitor cell functions in leukemogenesis. Leukemia. 2015; 29:1847–1856. [PubMed: 25801914]

Chen CW, Koche RP, Sinha AU, Deshpande AJ, Zhu N, Eng R, Doench JG, Xu H, Chu SH, Qi J, et al. DOT1L inhibits SIRT1-mediated epigenetic silencing to maintain leukemic gene expression in MLL-rearranged leukemia. Nature medicine. 2015; 21:335–343.

Chi P, Allis CD, Wang GG. Covalent histone modifications--miswritten, misinterpreted and mis-erased in human cancers. Nat Rev Cancer. 2010; 10:457–469. [PubMed: 20574448]

Eppert K, Takenaka K, Lechman ER, Waldron L, Nilsson B, van Galen P, Metzeler KH, Poeppl A, Ling V, Beyene J, et al. Stem cell gene expression programs influence clinical outcome in human leukemia. Nature medicine. 2011; 17:1086–1093.

Genovese G, Kahler AK, Handsaker RE, Lindberg J, Rose SA, Bakhoum SF, Chambert K, Mick E, Neale BM, Fromer M, et al. Clonal hematopoiesis and blood-cancer risk inferred from blood DNA sequence. The New England journal of medicine. 2014; 371:2477–2487. [PubMed: 25426838]

Guo X, Wang L, Li J, Ding Z, Xiao J, Yin X, He S, Shi P, Dong L, Li G, et al. Structural insight into autoinhibition and histone H3-induced activation of DNMT3A. Nature. 2015; 517:640–644. [PubMed: 25383530]

Heuser M, Yun H, Berg T, Yung E, Argiropoulos B, Kuchenbauer F, Park G, Hamwi I, Palmqvist L, Lai CK, et al. Cell of origin in AML: susceptibility to MN1-induced transformation is regulated by the MEIS1/AbdB-like HOX protein complex. Cancer cell. 2011; 20:39–52. [PubMed: 21741595]

Holz-Schietinger C, Matje DM, Reich NO. Mutations in DNA methyltransferase (DNMT3A) observed in acute myeloid leukemia patients disrupt processive methylation. The Journal of biological chemistry. 2012; 287:30941–30951. [PubMed: 22722925]

Huang Y, Sitwala K, Bronstein J, Sanders D, Dandekar M, Collins C, Robertson G, MacDonald J, Cezard T, Bilenky M, et al. Identification and characterization of Hoxa9 binding sites in hematopoietic cells. Blood. 2012; 119:388–398. [PubMed: 22072553]

Jaiswal S, Fontanillas P, Flannick J, Manning A, Grauman PV, Mar BG, Lindsley RC, Mermel CH, Burtt N, Chavez A, et al. Age-related clonal hematopoiesis associated with adverse outcomes. The New England journal of medicine. 2014; 371:2488–2498. [PubMed: 25426837]

Jones PA. Functions of DNA methylation: islands, start sites, gene bodies and beyond. Nature reviews Genetics. 2012; 13:484–492.

Kim SJ, Zhao H, Hardikar S, Singh AK, Goodell MA, Chen T. A DNMT3A mutation common in AML exhibits dominant-negative effects in murine ES cells. Blood. 2013; 122:4086–4089. [PubMed: 24167195]

Krivtsov AV, Twomey D, Feng Z, Stubbs MC, Wang Y, Faber J, Levine JE, Wang J, Hahn WC, Gilliland DG, et al. Transformation from committed progenitor to leukaemia stem cell initiated by MLL-AF9. Nature. 2006; 442:818–822. [PubMed: 16862118]

Lara-Astiaso D, Weiner A, Lorenzo-Vivas E, Zaretsky I, Jaitin DA, David E, Keren-Shaul H, Mildner A, Winter D, Jung S, et al. Immunogenetics. Chromatin state dynamics during blood formation. Science (New York, NY. 2014; 345:943–949.

Ley TJ, Ding L, Walter MJ, McLellan MD, Lamprecht T, Larson DE, Kandoth C, Payton JE, Baty J, Welch J, et al. DNMT3A mutations in acute myeloid leukemia. The New England journal of medicine. 2010; 363:2424–2433. [PubMed: 21067377]

Li Y, Wen H, Xi Y, Tanaka K, Wang H, Peng D, Ren Y, Jin Q, Dent SY, Li W, et al. AF9 YEATS domain links histone acetylation to DOT1L-mediated H3K79 methylation. Cell. 2014; 159:558–571. [PubMed: 25417107]

Mayle A, Yang L, Rodriguez B, Zhou T, Chang E, Curry CV, Challen GA, Li W, Wheeler D, Rebel VI, Goodell MA. Dnmt3a loss predisposes murine hematopoietic stem cells to malignant transformation. Blood. 2015; 125:629–638. [PubMed: 25416277]

Noh KM, Wang H, Kim HR, Wenderski W, Fang F, Li CH, Dewell S, Hughes SH, Melnick AM, Patel DJ, et al. Engineering of a Histone-Recognition Domain in Dnmt3a Alters the Epigenetic Landscape and Phenotypic Features of Mouse ESCs. Molecular cell. 2015; 59:89–103. [PubMed: 26073541]

Patel JP, Gonen M, Figueroa ME, Fernandez H, Sun Z, Racevskis J, Van Vlierberghe P, Dolgalev I, Thomas S, Aminova O, et al. Prognostic relevance of integrated genetic profiling in acute myeloid leukemia. The New England journal of medicine. 2012; 366:1079–1089. [PubMed: 22417203]

Rada-Iglesias A, Bajpai R, Swigut T, Brugmann SA, Flynn RA, Wysocka J. A unique chromatin signature uncovers early developmental enhancers in humans. Nature. 2011; 470:279–283. [PubMed: 21160473]

Russler-Germain DA, Spencer DH, Young MA, Lamprecht TL, Miller CA, Fulton R, Meyer MR, Erdmann-Gilmore P, Townsend RR, Wilson RK, Ley TJ. The R882H DNMT3A mutation associated with AML dominantly inhibits wild-type DNMT3A by blocking its ability to form active tetramers. Cancer cell. 2014; 25:442–454. [PubMed: 24656771]

Schmidl C, Klug M, Boeld TJ, Andreesen R, Hoffmann P, Edinger M, Rehli M. Lineage-specific DNA methylation in T cells correlates with histone methylation and enhancer activity. Genome research. 2009; 19:1165–1174. [PubMed: 19494038]

Schubeler D. Function and information content of DNA methylation. Nature. 2015; 517:321–326. [PubMed: 25592537]

Shih AH, Abdel-Wahab O, Patel JP, Levine RL. The role of mutations in epigenetic regulators in myeloid malignancies. Nat Rev Cancer. 2012; 12:599–612. [PubMed: 22898539]

Shih AH, Jiang Y, Meydan C, Shank K, Pandey S, Barreyro L, Antony-Debre I, Viale A, Socci N, Sun Y, et al. Mutational cooperativity linked to combinatorial epigenetic gain of function in acute myeloid leukemia. Cancer cell. 2015; 27:502–515. [PubMed: 25873173]

Shlush LI, Zandi S, Mitchell A, Chen WC, Brandwein JM, Gupta V, Kennedy JA, Schimmer AD, Schuh AC, Yee KW, et al. Identification of pre-leukaemic haematopoietic stem cells in acute leukaemia. Nature. 2014; 506:328–333. [PubMed: 24522528]

Wang GG, Cai L, Pasillas MP, Kamps MP. NUP98-NSD1 links H3K36 methylation to Hox-A gene activation and leukaemogenesis. Nature cell biology. 2007; 9:804–812. [PubMed: 17589499]

Wang GG, Pasillas MP, Kamps MP. Meis1 programs transcription of FLT3 and cancer stem cell character, using a mechanism that requires interaction with Pbx and a novel function of the Meis1 C-terminus. Blood. 2005; 106:254–264. [PubMed: 15755900]

Wang GG, Pasillas MP, Kamps MP. Persistent transactivation by meis1 replaces hox function in myeloid leukemogenesis models: evidence for co-occupancy of meis1-pbx and hox-pbx complexes on promoters of leukemia-associated genes. Molecular and cellular biology. 2006; 26:3902–3916. [PubMed: 16648484]

Wang GG, Song J, Wang Z, Dormann HL, Casadio F, Li H, Luo JL, Patel DJ, Allis CD. Haematopoietic malignancies caused by dysregulation of a chromatin-binding PHD finger. Nature. 2009; 459:847–851. [PubMed: 19430464]

Wong P, Iwasaki M, Somervaille TC, So CW, Cleary ML. Meis1 is an essential and rate-limiting regulator of MLL leukemia stem cell potential. Genes & development. 2007; 21:2762–2774. [PubMed: 17942707]

Xiang P, Wei W, Lo C, Rosten P, Hou J, Hoodless PA, Bilenky M, Bonifer C, Cockerill PN, Kirkpatrick A, et al. Delineating MEIS1 cis-regulatory elements active in hematopoietic cells. Leukemia. 2014; 28:433–436. [PubMed: 24097337]

Xie M, Lu C, Wang J, McLellan MD, Johnson KJ, Wendl MC, McMichael JF, Schmidt HK, Yellapantula V, Miller CA, et al. Age-related mutations associated with clonal hematopoietic expansion and malignancies. Nature medicine. 2014; 20:1472–1478.

Xu J, Wang YY, Dai YJ, Zhang W, Zhang WN, Xiong SM, Gu ZH, Wang KK, Zeng R, Chen Z, Chen SJ. DNMT3A Arg882 mutation drives chronic myelomonocytic leukemia through disturbing gene expression/DNA methylation in hematopoietic cells. Proceedings of the National Academy of Sciences of the United States of America. 2014; 111:2620–2625. [PubMed: 24497509]

Yan XJ, Xu J, Gu ZH, Pan CM, Lu G, Shen Y, Shi JY, Zhu YM, Tang L, Zhang XW, et al. Exome sequencing identifies somatic mutations of DNA methyltransferase gene DNMT3A in acute monocytic leukemia. Nature genetics. 2011; 43:309–315. [PubMed: 21399634]

Yang L, Rau R, Goodell MA. DNMT3A in haematological malignancies. Nat Rev Cancer. 2015; 15:152–165. [PubMed: 25693834]

Zhang J, Wang J, Liu Y, Sidik H, Young KH, Lodish HF, Fleming MD. Oncogenic Kras-induced leukemogeneis: hematopoietic stem cells as the initial target and lineage-specific progenitors as the potential targets for final leukemic transformation. Blood. 2009; 113:1304–1314. [PubMed: 19066392]

SIGNIFICANCE

Recurrent *DNMT3A* mutations at Arg882 are found in hematological malignancies and disorders; however, due to a lack of relevant disease models, molecular mechanisms by which *DNMT3A* mutations influence leukemogenesis remain largely undefined. Through establishment and characterization of murine leukemia and leukemia stem cell models, we show that *DNMT3A*^{R882H} mutation potentiates transactivation of stemness genes required for acute leukemogenicity. Integrated epigenomic profiling of murine models further reveals the underlying epigenetic alterations induced by DNMT3A^{R882H}, which are enriched at gene-regulatory sites and resemble those seen in human patients. Pharmacological inhibition of Dot1l suppresses DNMT3A^{R882H}-associated gene activation and acute leukemogenesis. Our findings not only promote mechanistic understandings of *DNMT3A* mutation-associated clonal and malignant hematopoiesis but also provide a therapeutic avenue for *DNMT3A*-mutated leukemias.

Highlights

- DNMT3A^{R882H} promotes acute leukemogenicity in the presence of mutant NRAS
- DNMT3A^{R882H} induces focal DNA hypomethylation at cis-elements of key stemness genes
- DNMT3A^{R882H} potentiates stemness gene expression via enhancer/promoter activation
- DNMT3A^{R882H}-induced gene activation programs are sensitive to Dot1l blockade

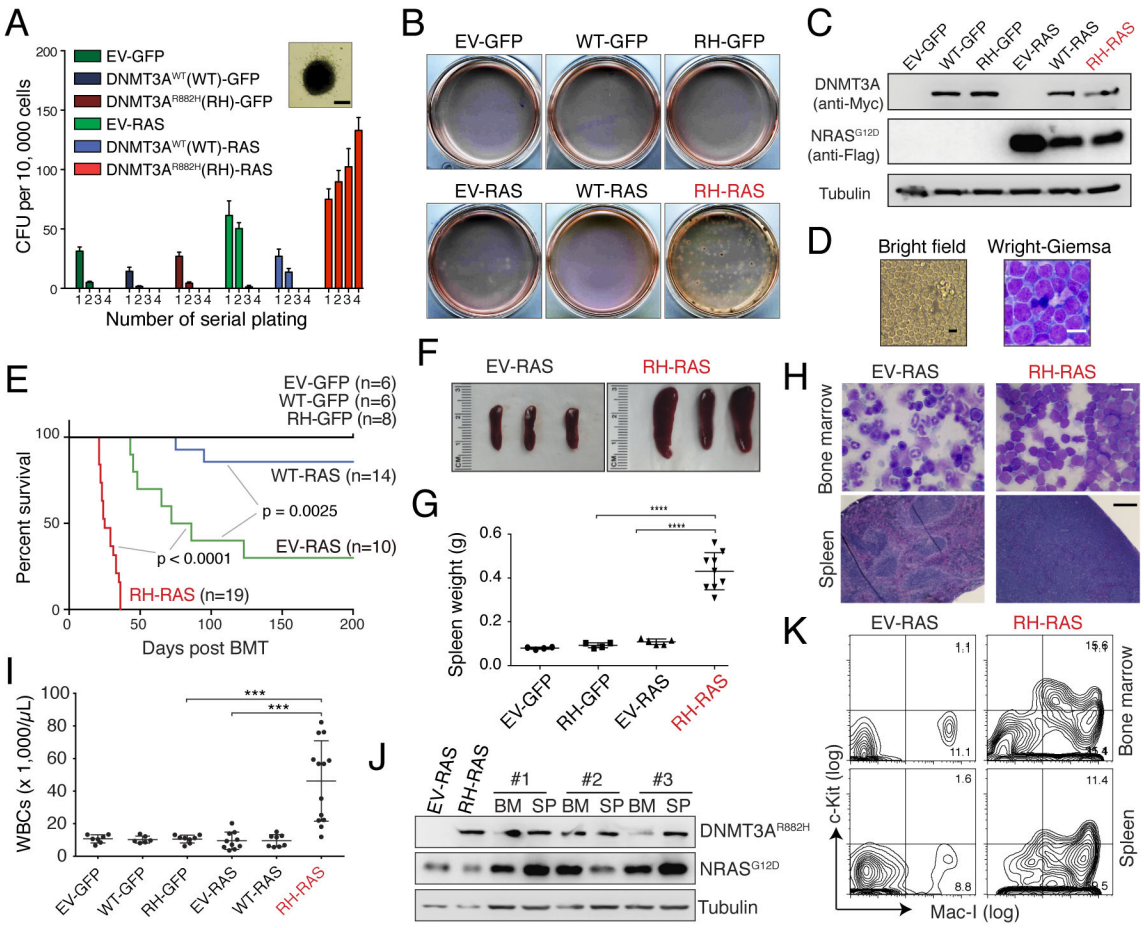

Figure 1. DNMT3A^{R882H} acts in concert with mutant RAS to transform murine HSPCs ex vivo and induce AMLs in vivo

(A) Colony-forming unit (CFU) assay using murine HSPCs expressing empty control (EV), wild-type (WT) or R882H mutant (RH) DNMT3A in combination with GFP or NRAS^{G12D} (RAS) Insert, a typical colony expressing RH-RAS at the 4th replating. Scale bar, 1 mm.

(B) Images of CFU assay at the 4th replating.

(C) Immunoblot of DNMT3A (Myc-tagged) and NRAS (Flag-tagged) in HSPCs post-infection.

(D) Microscopic image and Wright-Giemsa staining of RH-RAS-coexpressing cells derived from the 4th replating after long-term culture with the SCF cytokine in vitro. Scale bar, 10 μm.

(E) Kaplan-Meier survival curve of mice after bone marrow transplantation (BMT) of HSPCs freshly transduced with indicated genes. The p values were calculated by log-rank test.

(F–G) Spleen size (panel F, n = 3) and weight (panel G, n = 4–7) of indicated cohorts 3–4 weeks post-BMT. The p values were calculated by Student's t-test.

(H) Wright–Giemsa staining of bone marrow (upper) and H&E staining of spleen (bottom) of indicated cohorts 4 weeks post-BMT. Scale bar, 10 μm (upper) and 200 μm (bottom).

(I) White blood cell (WBC) counts in peripheral blood of indicated cohorts (n = 6–13) 4 weeks post-BMT. The p values were calculated by Student's t-test.
(J) Immunoblot of DNMT3A (Myc) and NRAS (Flag) proteins in bone marrow (BM) and spleen (SP) cells from mice with leukemia induced by RH-RAS coexpression. The first 2 lanes were loaded with samples of in vitro infected HSPCs.
(K) FACS analysis of Mac-1 and c-Kit with bone marrow and spleen cells of indicated cohorts 4 weeks post-BMT.
Error bar, +/− SD; ***, $p < 0.001$; ****, $p < 0.0001$.
See also Figure S1 and Table S1.

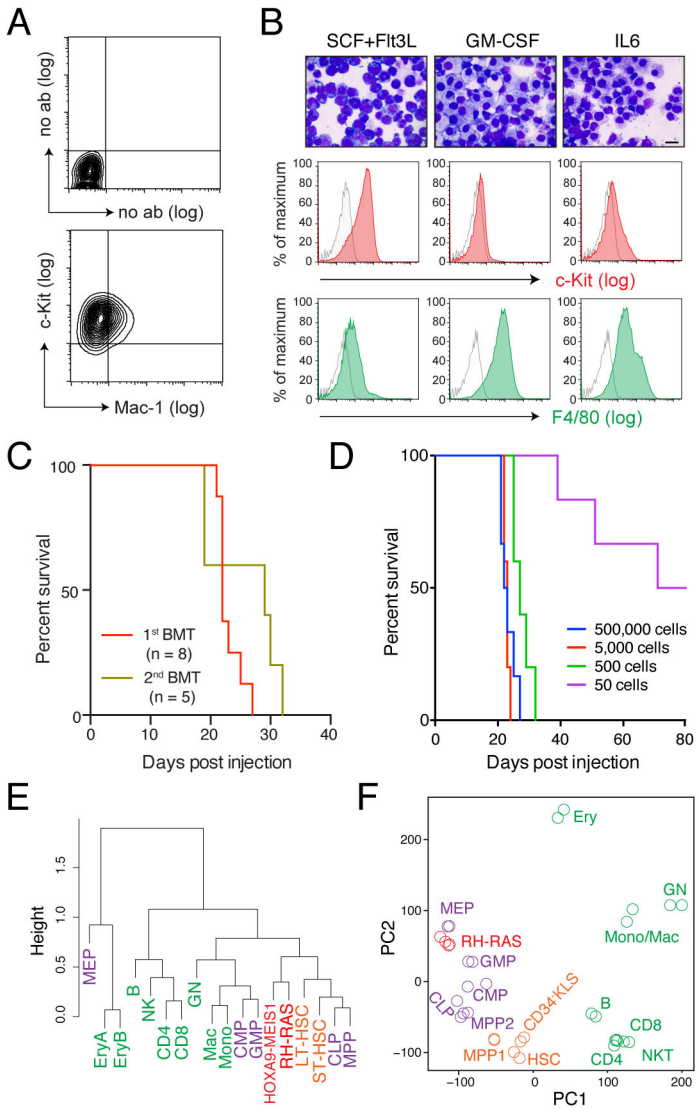

Figure 2. R882-mutated DNMT3A establishes leukemia-initiating stem cells (LSCs) ex vivo in the presence of activated RAS

(A) FACS analysis of in vitro immortalized progenitors by RH-RAS using a liquid culture system.

(B) Wright–Giemsa staining (upper) and FACS analysis of RH-RAS-immortalized progenitors 14 days post-cultivation with indicated cytokines. FACS control, non-specific IgG (grey, open); Scale bar, 10 μm.

(C) Kaplan-Meier curve of mice receiving primary or secondary BMT with RH-RAS induced leukemia.

(D) Kaplan-Meier curve of mice (n = 5–6) receiving BMT of the indicated numbers of RH-RAS immortalized cells.

(E) Hierarchical clustering of genome-wide H3K4me1 profiles of LSCs$^{RH\text{-}RAS}$, AML-causing LSC lines produced by overexpressed HOXA9 plus MEIS1 (HOXA9-MEIS1), and various normal blood cell types. LT-HSC, long-term HSC; ST-HSC, short-term HSC; MPP,

multipotent progenitor; CMP, common myeloid progenitor; CLP, common lymphoid progenitor; GMP, granulocyte-monocyte progenitor; MEP, megakaryocyte-erythroid progenitor; Mac, macrophage; Mono, monocyte; GN, granulocyte; B, $B220^{+}/CD19^{+}$ B-cell; CD4/8, $CD4/8^{+}$ T-cell; NK, natural killer cell; EryA and EryB, $Ter119^{+}/CD71^{+}$ erythroid cell with high and low forward scatter, respectively.

(F) Principal component (PC) analysis of transcriptome profiles of $LSCs^{RH\text{-}RAS}$ and various normal blood cell types. Besides what is described in panel E, $CD34^{-}KLS$, $Cd34^{-}/c\text{-}Kit^{+}/Lin^{-}/ScaI^{+}$ HSC; MPP1, $Flk2^{-}$ multipotent progenitor; MPP2, $Flk2^{+}$ multipotent progenitor; NKT, natural killer T-cell; Ery, erythroid cell.

See also Figure S2.

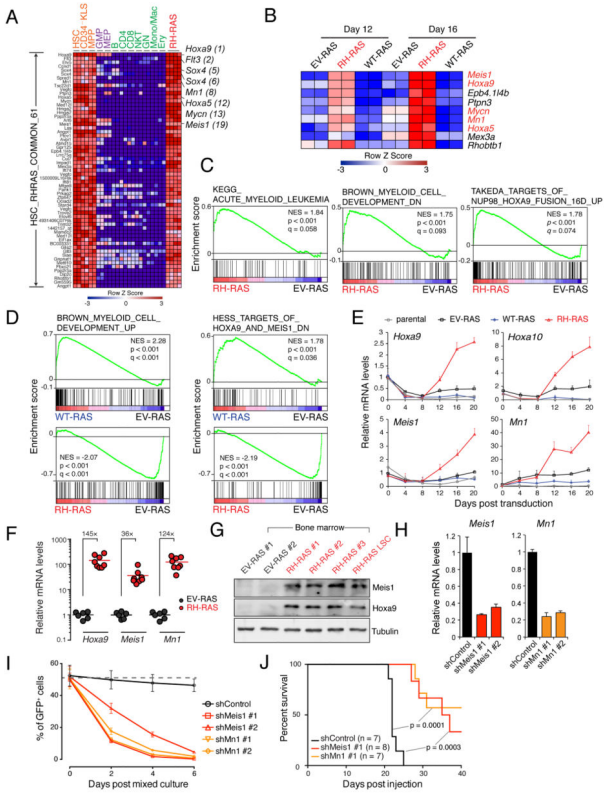

Figure 3. DNMT3A^{R882H} potentiates aberrant activation of stemness genes including a critical *Meis1-Mn1-Hoxa* regulatory node

(A) Heatmap of 61 probes (54 genes) showing unique expression in both self-renewing HSPCs (HSC, Cd34^{-}KLS and MPP) and LSCs$^{RH\text{-}RAS}$ but not in differentiating (purple) or mature (green) blood cell types. Probes are ranked by higher expression in LSCs$^{RH\text{-}RAS}$ relative to differentiating and mature cells. Example genes are highlighted along with their respective rankings.

(B) Of the 54 self-renewal genes, genes showing consistently higher expression in HSPCs 12 and 16 days post-transduction of RH-RAS relative to EV-RAS.

(C) GSEA shows enrichment of AML-associated genes (left), genes downregulated upon myeloid differentiation (middle) and NUP98-HOXA9 targets (right) in HSPCs with RH-RAS versus EV-RAS.

(D) GSEA shows enrichment of differentiation gene sets in WT-RAS or RH-RAS HSPCs relative to EV-RAS. Left, myeloid differentiation genes; right, genes downregulated upon activation of HOXA9 and MEIS1.

(E) RT-qPCR of indicated genes in murine HSPCs post-transduction of EV-RAS, WT-RAS or RH-RAS.

(F) RT-qPCR of indicated genes in mouse bone marrow 21 days post-BMT of HSPCs with EV-RAS (n = 6) or RH-RAS (n = 8).

(G) Immunoblot of Meis1 and Hoxa9 in bone marrow of mice 21 days post-BMT of HSPCs with EV-RAS or RH-RAS. The last lane was loaded with LSC$^{RH\text{-}RAS}$ samples.

(H) RT-qPCR showing shRNA-mediated *Meis1* or *Mn1* knockdown in LSCs$^{RH\text{-}RAS}$.

(I) Relative proliferation of indicated shRNA-expressing $LSCs^{RH\text{-}RAS}$ (GFP^+) versus parental cells (GFP^-). These GFP^- and GFP^+ cells were mixed in a 1:1 ratio at day 0, followed by measurement of % of GFP^+ cells.
(J) Kaplan-Meier curve of mice engrafted with indicated shRNA-expressing $LSCs^{RH\text{-}RAS}$. The p values were calculated by log-rank test.
Error bar, +/− SD.
See also Figure S3 and Table S2.

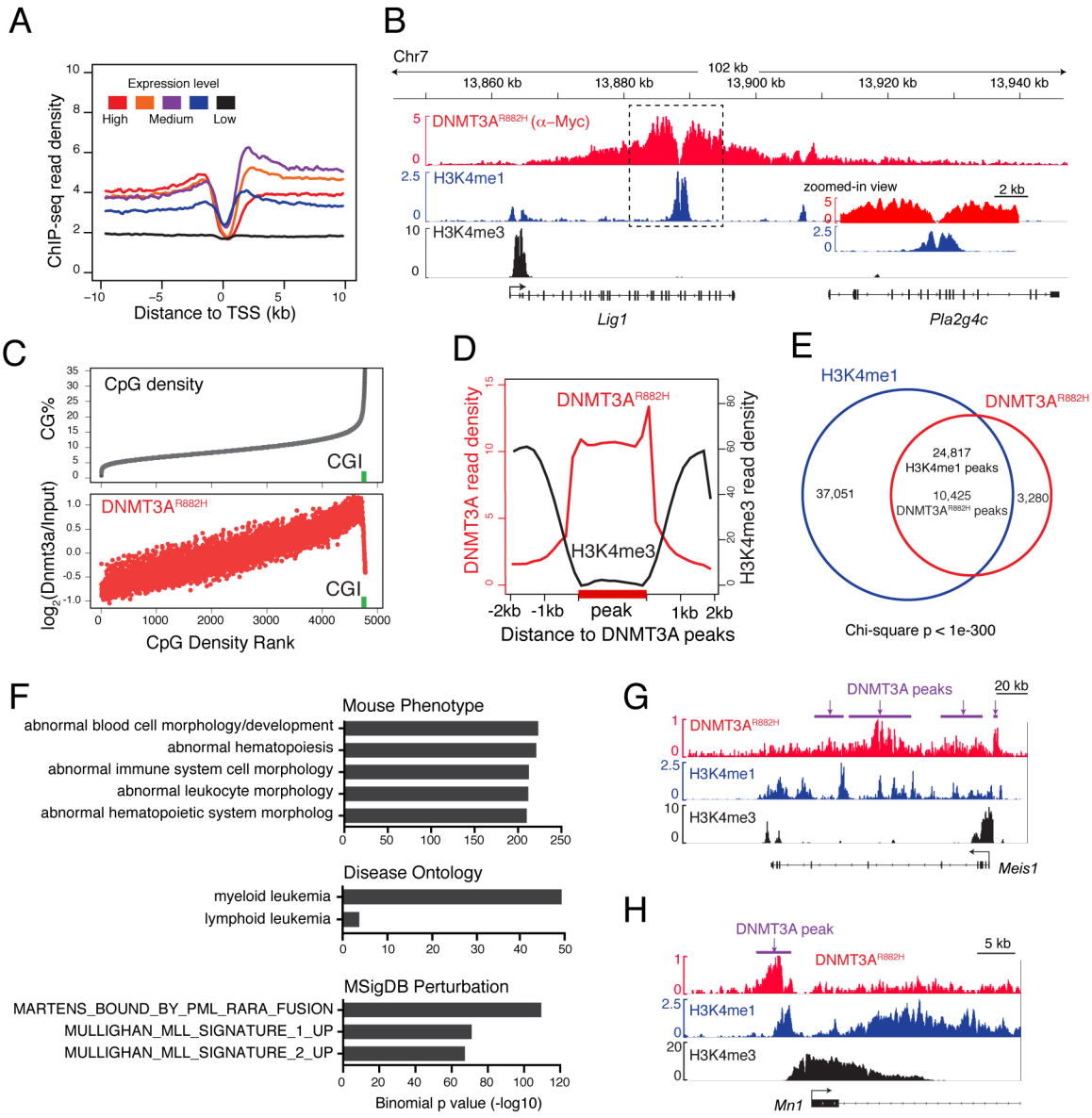

Figure 4. ChIP-Seq reveals chromatin context-dependent binding of R882-mutated DNMT3A to genomic regions, including stemness genes such as a *Meis1-Mn1-Hoxa* node

(A) DNMT3A^{R882H} ChIP-Seq profiles across transcription start site (TSS) of genes with different expression levels in LSCs$^{RH\text{-}RAS}$.

(B) Example ChIP-Seq profiles for DNMT3A^{R882H}, H3K4me1 and H3K4me3 at the *Lig1* gene. Box, a zoomed-in view of dashed box region showing overlap of DNMT3A^{R882H} and H3K4me1 peaks.

(C) Correlation of DNMT3A^{R882H} binding and CpG density. Shown is % of CpG density (grey) and DNMT3A^{R882H} ChIP-Seq reads (red) at 1-kb windows of the entire genome ranked by CpG density. Green square, CpG island (CGI).

(D) Plot of averaged DNMT3A^{R882H} (red) and H3K4me3 (black) ChIP-Seq signals at DNMT3A^{R882H} peaks (labeled in bold on x-axis) and surrounding regions (+/−2 kb).

(E) Venn diagram shows significant overlap of DNMT3A^{R882H} and H3K4me1 peaks in LSCs$^{RH\text{-}RAS}$.

(F) Genomic Regions Enrichment of Annotations Tool (GREAT) analysis shows enrichment of indicated gene signatures among DNMT3A^{R882H} peaks.

(G–H) ChIP-Seq profiles of DNMT3A^{R882H}, H3K4me1 and H3K4me3 at *Meis1* (panel G) and *Mn1* (panel H). Purple bars, DNMT3A^{R882H} peak calls.

See also Figure S4 and Table S3.

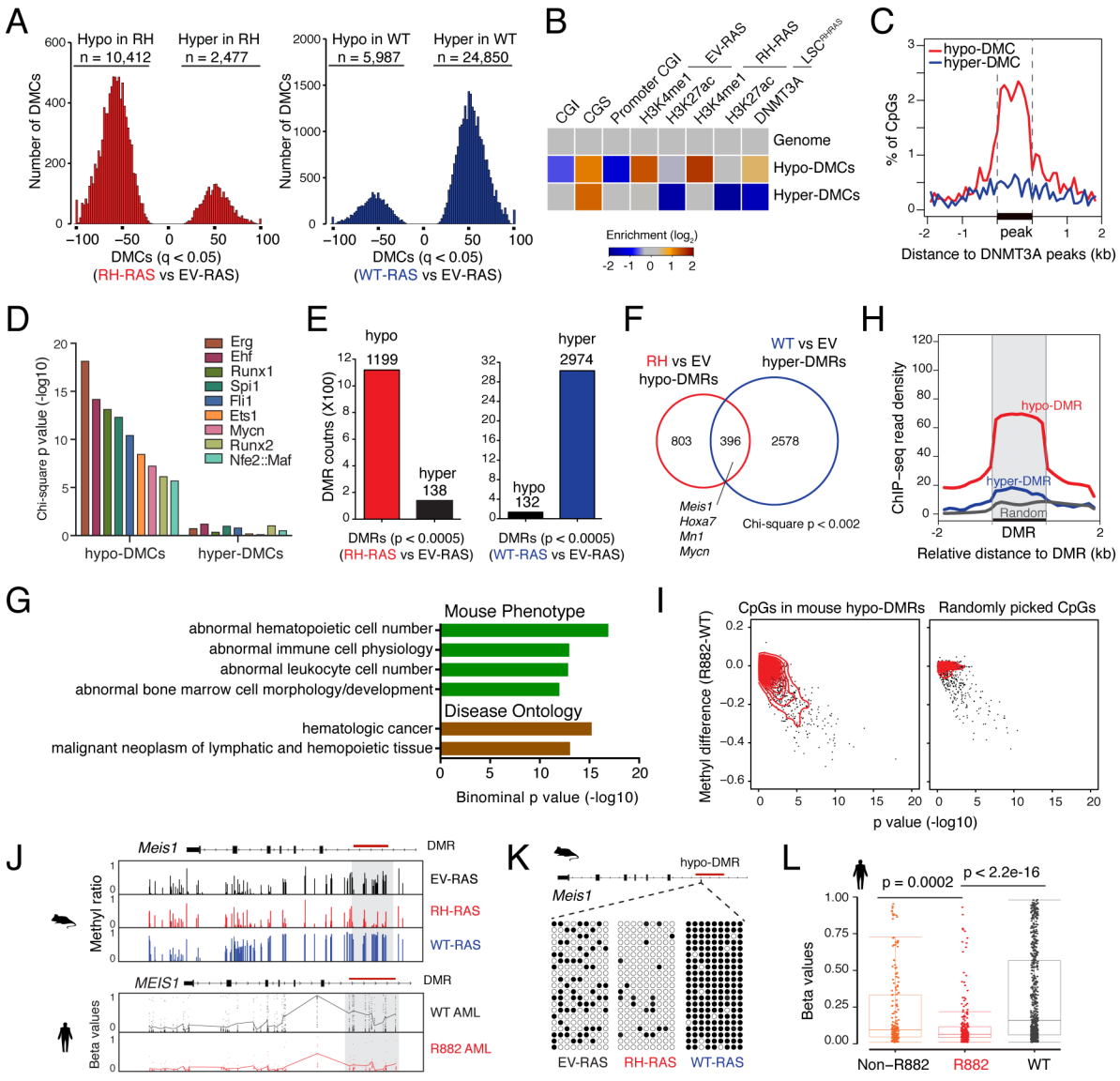

Figure 5. DNMT3A^{R882H} induces focal CpG hypomethylations enriched at H3K4me1-demarcated, gene-regulatory sites in HSPCs

(A) Distribution of DMCs in the genome of murine HSPCs transduced with RH-RAS or WT-RAS, relative to EV-RAS.

(B) Heatmap showing enrichment of DNMT3A^{R882H}-associated DMCs at indicated genomic regions or ChIP-Seq peaks in comparison to genome average. The enrichment value was calculated as $\log_2$(observed/expected) of the DMC numbers. CGI, CpG island; CGS, CpG shore.

(C) Distribution of DNMT3A^{R882H}-associated DMCs across DNMT3A^{R882H} ChIP-Seq peaks (shown in a bold bar on x-axis). Y-axis shows % of DMCs located at 100-bp window of genomic regions centered on DNMT3A^{R882H} peaks.

(D) Enrichment of indicated TF binding motifs in DNMT3A^{R882H}-associated hypo-DMCs and hyper-DMCs.

(E) Summary of DMRs identified in the HSPCs with RH-RAS or WT-RAS, relative to EV-RAS.
(F) Venn diagram showing overlap of DNMT3A^{R882H} and DNMT3A^{WT}-associated DMRs.
(G) GREAT annotation of DNMT3A^{R882H}-associated hypo-DMRs.
(H) H3K4me1 profiles at DNMT3A^{R882H}-associated hypo-DMRs, hyper-DMRs, and random control regions. Plotted across DMRs (labeled in a bold line on x-axis) were averaged H3K4me1 ChIP-Seq read densities in EV-RAS cells.
(I) Scatter plots showing methylation changes of selected CpGs in human AMLs with *DNMT3A* R882 mutation relative to *DNMT3A* WT AMLs. Mean methylation differences (y-axis) and p value (x-axis) for each CpG between two AML patient groups were plotted. Left, CpGs in the human genome homologous to DNMT3A^{R882H}-associated hypo-DMRs identified in murine HSPCs; right, randomly picked CpG controls.
(J) DNA methylation profiles of *Meis1* in indicated murine HSPCs and *MEIS1* in human AMLs with WT (n = 50) or R882-mutated (n = 20) *DNMT3A.* Faded points show individual CpG methylation beta values and connected lines indicate the mean methylation levels at each CpG site. Grey box, a hypo-DMR in intron 6.
(K) Bisulfite sequencing of the *Meis1* intron 6 DMR in indicated murine HSPC samples.
(L) Box plots of methylation beta values of all CpGs (shown as dots in boxplot) at *MEIS1* intron 6 in human AMLs with R882-mutated *DNMT3A* (n = 20) relative to AMLs with either non-R882 mutated (n = 15) or WT (n = 50) *DNMT3A*. Horizontal line, median; box, interquartile range; whiskers extend to 1.5× the interquartile range. The p values were calculated by Mann-Whitney U test.
See also Figure S5 and Table S4 and S5.

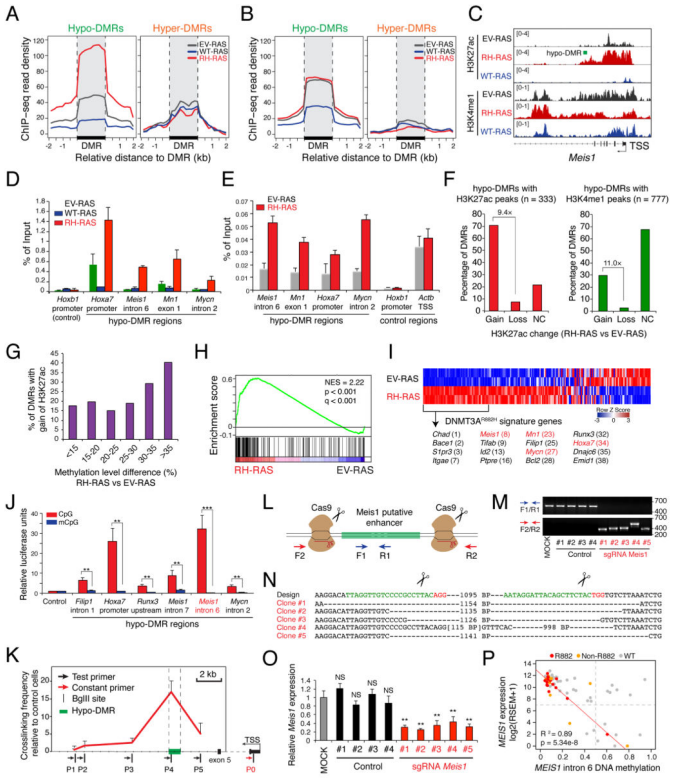

Figure 6. DNMT3A^{R882H}-associated hypo-DMRs gain epigenetic alterations associated with gene activation

(A–B) H3K27ac (panel A) and H3K4me1 (panel B) profiles at DNMT3A^{R882H}-associated DMRs (bold on x-axis) and the surrounding regions. Averaged ChIP-Seq read densities in HSPCs with EV-RAS, RH-RAS or WT-RAS were plotted.

(C) H3K27ac and H3K4me1 profiles at *Meis1* intron 6 in indicated HSPCs. Green bar, hypo-DMR.

(D–E) ChIP-qPCR of H3K27ac (panel D) and p300 binding (panel E) at hypo-DMRs in indicated HSPCs.

(F) Percentage of DNMT3A^{R882H}-associated hypo-DMRs showing indicated H3K27ac changes in HSPCs with RH-RAS versus EV-RAS. Gain, increased H3K27ac; Loss, reduced H3K27ac; NC, no significant H3K27ac change. The total DMRs used for calculation were hypo-DMRs carrying H3K27ac (left) or H3K4me1 (right) in at least one cell condition.

(G) Percentage of DNMT3A^{R882H}-associated hypo-DMRs (n = 1,199) showing H3K27ac gain in HSPCs with RH-RAS versus EV-RAS, when these hypo-DMRs are divided based on degree of DNA methylation reduction (x-axis) shown in the same samples.

(H) GSEA shows that genes with gain of H3K27ac at hypo-DMRs are enriched in HSPCs 16 days post-transduction of RH-RAS, relative to EV-RAS.

(I) Heatmap shows expression of genes in panel H ranked by higher expression in HSPCs with RH-RAS, relative to EV-RAS. The significantly upregulated genes in RH-RAS HSPCs are defined as "DNMT3A^{R882H} signature genes" (n = 57), with selected ones listed along with their respective rankings (bottom).

(J) Quantification of expression-enhancing activity of DNMT3A^{R882H}-associated hypo-DMRs with the embedded CpGs either non-methylated (CpG) or methylated (mCpG) using a CpG-free luciferase reporter system. The reporter without any DMR insertion was used as control. The p values were calculated by Student's t-test.

(K) 3C assay shows looping interaction of the *Meis1* intron 6 hypo-DMR (P4) to gene promoter (P0), relative to other tested sites.

(L–M) Scheme (panel L) and PCR validation (panel M) of CRISPR/Cas9-mediated deletion of the *Meis1* intron 6 DMR. MOCK, parental LSC^{RH-RAS}; Control, no sgRNA; sgMeis1, a pair of sgRNAs that target the DMR boundaries.

(N) Sequencing of the genomic PCR products from F2/R2 primers shows CRISPR/Cas9-induced deletion of the *Meis1* intron 6 DMR.

(O) Expression levels of *Meis1* in LSC^{RH-RAS} lines shown in panel M. The p values were calculated by Student's t-test by comparing to MOCK.

(P) Impact of DNA methylation levels in *MEIS1* intron 6 in cytogenetically normal human AMLs grouped by *DNMT3A* WT (n = 45), non-R882 (n = 13) and R882 mutations (n =16). Plotted were mean methylation beta values of CpGs at *MEIS1* intron 6 and log2-transformed expression values of RNA-Seq by Expectation-Maximization (RSEM). R^2 and p values shown were determined with data of R882-mutant AMLs.

Error bar, +/− SD; **, $p < 0.01$; ***, $p < 0.001$; NS, not significant.

See also Figure S6 and Table S4 and S6.

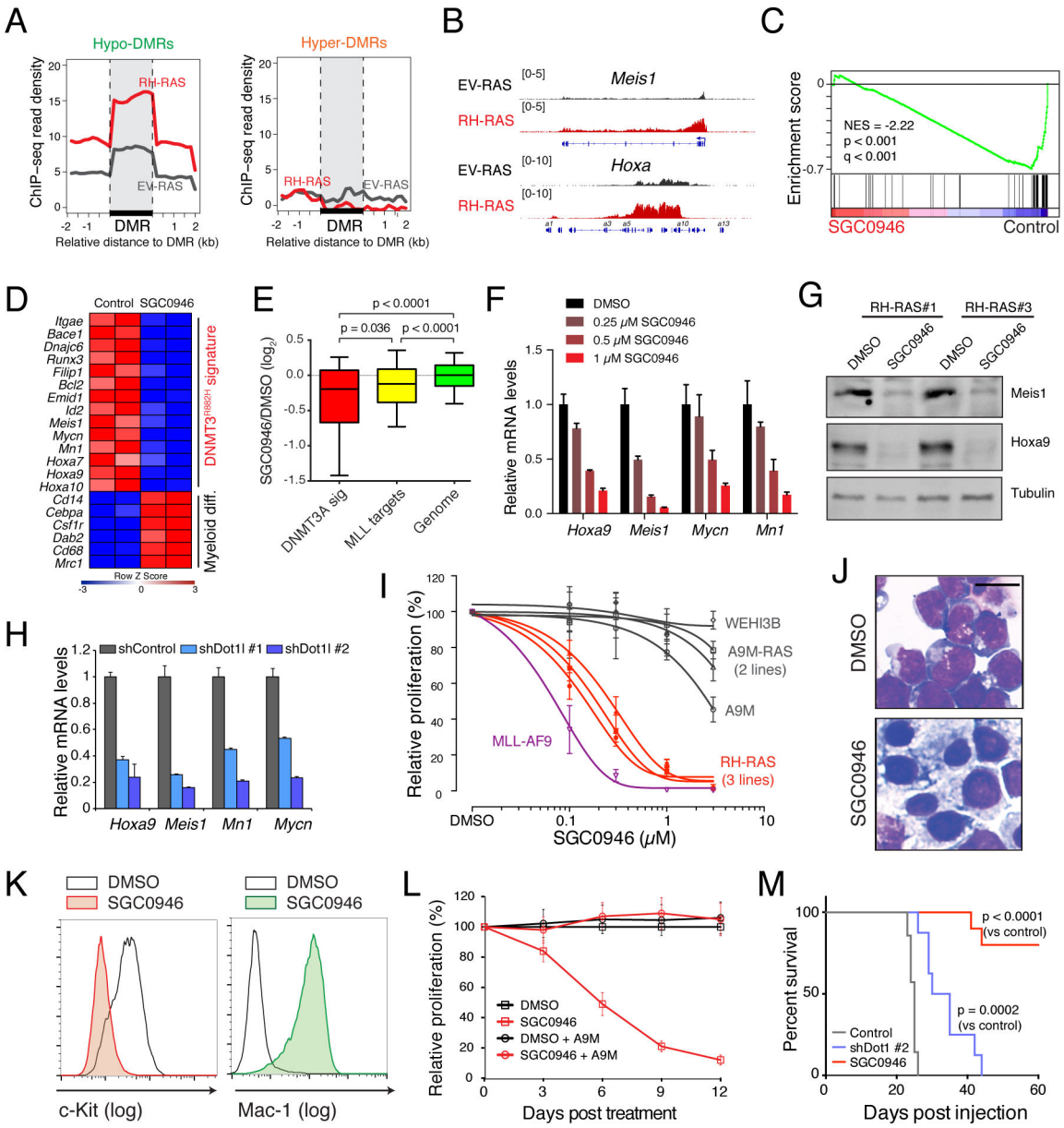

Figure 7. Dot1l inhibition reverses DNMT3A^{R882H}-mediated aberrant transactivation of stem cell genes, thereby suppressing acute leukemogenicity

(A) Averaged H3K79me2 ChIP-Seq signals at DNMT3A^{R882H}-associated hypo-DMRs and hyper-DMRs in HSPCs with RH-RAS or EV-RAS.

(B) H3K79me2 profiles at *Meis1* and *Hoxa* in indicated HSPCs.

(C) GSEA shows downregulation of DNMT3A^{R882H} signature genes in LSCs^{RH-RAS} post-treatment with 1 μM SGC0946 for 4 days.

(D) Heatmap shows downregulation of DNMT3A^{R882H} signature genes and upregulation of myeloid differentiation genes in SGC0946-treated LSCs^{RH-RAS} versus mock-treated.

(E) Boxplots show relative expression of DNMT3A signature genes (n = 54), MLL-AF9 gene targets (n = 129) and all genes in the genome in SGC0946-treated LSCs^{RH-RAS},

relative to mock-treated. Horizontal line, median; box, interquartile range; whiskers, 10 to 90 percentiles. The p values were calculated by Mann-Whitney U test.

(F–G) RT-qPCR (panel F) and immunoblot (panel G) of indicated genes and proteins in $LSCs^{RH\text{-}RAS}$ 6 days post-treatment with SGC0946.

(H) Expression of indicated genes in $LSCs^{RH\text{-}RAS}$ transduced with *Dot1l* shRNAs or vector control.

(I) Relative growth of $LSCs^{RH\text{-}RAS}$ and other AML lines established by MLL-AF9, Hoxa9 plus Meis1 (A9M), A9M plus $NRAS^{G12D}$ (A9M-RAS), and Hoxb8 plus Meis2 (WEHI3B) after a 12-day treatment with SGC0946 versus DMSO.

(J–K) Wright–Giemsa staining (panel J) and FACS analysis (panel K) of $LSCs^{RH\text{-}RAS}$ 6 days post-treatment with DMSO or 1 μM SGC0946. Scale bar, 10 μm.

(L) Effect of SGC0946 on growth of $LSCs^{RH\text{-}RAS}$ transduced with vector or Hoxa9 plus Meis1 (A9M). Relative proliferation was normalized to DMSO-treated cells.

(M) Survival of mice engrafted with $LSCs^{RH\text{-}RAS}$, either mock-treated, stably transduced with a *Dot1l* shRNA, or pre-treated with 1 μM SGC0946 ex vivo for 6 days. The p values were calculated by log-rank test.

Error bar, +/− SD.

See also Figure S7 and Table S6.